Supporting Information

Biophysical Evaluation of Protein Structural Flexibility on Ligand Biorecognition in Solid Solution

Fei Ding[acd] and Wei Peng*[ab]

[a] *College of Agriculture and Plant Protection, Qingdao Agricultural University, Qingdao 266109, China*

[b] *College of Food Science and Engineering, Qingdao Agricultural University, Qingdao 266109, China*

[c] *Department of Chemistry, China Agricultural University, Beijing 100193, China*

[d] *Department of Biological Engineering, Massachusetts Institute of Technology, Cambridge, MA 02139, United States*

*Corresponding Author
Phone/fax: +86-29-87092367
E-mail: crystalw.peng@outlook.com, weipeng@cau.edu.cn

A Short Introduction to Triphenylmethane. Triphenylmethane compound is one of the most widely used synthetic colorants, and maybe C.I. Basic Green 4 (structure shown in Fig. 1) stands out as the best in the category. Chemically, triphenylmethane serves many purposes, for instance, it is used as a blue-green counterstain for microscopic analysis of cell biology and tissue samples.[1] In industry, triphenylmethane is generally employed to color various commodities, e.g. cosmetics, drugs, fur, glass, leather, paper, plastics, polishes, silk, soaps, stationery and wool.[2] Notably, C.I. Basic Green 4 has been proved to be especially efficacious in the prevention of various pathomycetes such as oomycete *Saprolegnia*, which infects fish eggs in commercial aquacultures.[3-5] Therefore, the fishermen frequently applied C.I. Basic Green 4 in great quantities to control branchiomycosis, ichthyophthiriasis and saprolegniasis for fish. Meanwhile, C.I. Basic Green 4 can often be added to the freshwater aquaria for disinfection that help to prolong the survival time during the transportation and storage process of fish and other aquatic products.[6] However, owing to its highly toxic and residual properties for aquaculture, along with the very slowly metabolic rate and long residual time in fish and environment, many government agencies, such as European Food Safety Authority, Food Safety Commission of Japan, Health Canada, U.S. Environmental Protection Agency, and U.S. Food and Drug Administration have prohibited the use of triphenylmethane on any aquatic species.[7-9] Furthermore, a number of studies reported so far indicate that triphenylmethane is a multi-organ toxin in mammalians.[10-15] Fernandes et al.[16] discovered that C.I. Basic Green 4 is carcinogenic to male *Wistar* rats, and Meyer and

Jorgenson[17] noticed conspicuous teratological effects in New Zealand white rabbits administered orally 0, 5, 10, and 20 mg kg^{-1} C.I. Basic Green 4 by gavage on days 6 through 18 of gestation. C.I. Basic Green 4 has also been found to be mutagenic in rats and mice, and it is highly cytotoxic to mammalian cells.[11,13] Nevertheless, it is relatively inexpensive, readily available, and highly efficacious, this compound possibly continued use in some United States fisheries and, in particular, it has yet been used extensively in several developing countries such as China which had less power in aquaculture and fishery management as the most effective antifungal agent.[18,19]

As Briggs[20] has noted, the pollutants in the environment (include agricultural and industrial commodities and water) can routinely be entered in the human body mainly through chronic exposure and food chain, thus impairing human's health. Moreover, the damages of these pollutants for humans are usually far from acute or immediate effects, but probably by bioaccumulation in different organs such as kidney, liver and spleen, namely chronic toxicity.[21-24] In view of its physicochemical and toxicological properties, together with successive emergence of reports about the determination of illegal triphenylmethane in a variety of commodities,[25-32] it is necessary to elaborate the biomolecular recognition event between triphenylmethane compound and the central biopolymer in the human body at the molecular scale. Under the protein-mediated environment, triphenylmethane has successfully been utilized as electrophile, heater ligand, photosensitizer and photo-to-heat converter, and meanwhile, the biointeraction of triphenylmethane with albumin from bovine serum

(BSA) has also been inspected preliminarily via spectroscopic techniques.[33-38] But the molecular recognition of triphenylmethane by homologous albumin from human serum (HSA) remains hazy, and in particular, the influences of the chemical on homologous mammalian protein's flexibility and dynamic feature in recognition process are yet unanswered.

Time-Resolved Fluorescence. Time-resolved fluorescence was examined with a FLS920 spectrometer (Edinburgh Instruments, UK), using the time-correlated single photon counting system with a hydrogen flash lamp excitation source, in air equilibrated solution at an ambient temperature. The excitation wavelength was 295 nm and the number of counts gathered in the channel of maximum intensity was 4,000. The instrument response function (IRF) was gauged exploiting Ludox to scatter light at the excitation wavelength. The data were analyzed with a nonlinear least-squares iterative method utilizing the Fluorescence Analysis Software Technology, which is a sophisticated software package designed by Edinburgh Photonics for the analysis of fluorescence and phosphorescence decay kinetics, IRF was deconvoluted from the experimental data, and the resolution limit after deconvolution was 0.2 ns. The value of χ^2 (0.9～1.2), the Durbin-Watson parameter (greater than 1.7), as well as a visual inspection of the residuals were used to assess how well the calculated decay fit the data. Average fluorescence lifetime (τ) for multiexponential function fittings were from the following relation:[39-41]

$$I(t) = \sum_i A_i e^{\frac{-t}{\tau_i}} \quad (1)$$

where τ_i are fluorescence lifetimes and A_i are their relative amplitudes, with i variable from 1 to 2.

Site-Specific Ligand. Binding location studies between albumin and triphenylmethane in the presence of four typical site markers (phenylbutazone, flufenamic acid and digitoxin) were executed using the fluorescence titration approach. The concentration of HSA and site markers were held in equimolar (1.0 μM), then triphenylmethane was added to the HSA-site markers mixtures. An excitation wavelength of 295 nm was chosen and the fluorescence emission wavelength was acquired from 300 to 450 nm.

Circular Dichroism. Far-UV CD spectra were collected with a Jasco-815 spectropolarimeter (Jasco, Japan) equipped with a microcomputer, the apparatus was sufficiently purged with 99.9% dry nitrogen gas before starting the instrument and then it is calibrated with d-10-camphorsulfonic acid. All the CD spectra were got at 298 K with a PFD-425S Peltier temperature controller attached to a water bath with an accuracy of $\pm$0.1 ^{o}C. Each spectrum was performed with use of a precision quartz cuvette of 1.0 cm path length and taken at wavelengths between 200 and 260 nm range that provides a signal extremely sensitive to small secondary conformational distortions. Every determination was the average of five successive scans encoded with 0.1 nm step resolution and recorded at a speed of 50 nm min^{-1} and response time of 1 s. All observed CD data were baseline subtracted for buffer and the estimation of the secondary structure elements was obtained by exploiting Jasco Spectra Manager II, which computes the different designations of secondary structures by comparison with CD spectra, determined from distinct proteins for which high-quality X-ray diffraction data are available.

Ligand Docking. *In silico* docking of the BSA-triphenylmethane complex was operated on SGI Fuel Visual Workstation. The crystal structure of BSA (entry codes 4JK4),[42-45] determined at a resolution 2.65 Å, was retrieved from the Brookhaven Protein Data Bank (http://www.rcsb.org/pdb). After being imported in the program Sybyl Version 7.3 (http://www.certara.com), BSA structure was carefully checked for atom and bond type correctness assignment. Hydrogen atoms were computationally added using the Sybyl Biopolymer and Build/Edit menus. To avoid negative acid/acid interactions and repulsive steric clashes, added hydrogen atoms were energy minimized with the Powell algorithm with 0.05 kcal mol^{-1} energy gradient convergence criteria for 1500 cycles, this procedure does not change positions to heavy atoms, and the potential of the three-dimensional structure of BSA was assigned according to the AMBER force field with Kollman all-atom charges.[46] The two-dimensional structure of triphenylmethane was downloaded from PubChem (http://pubchem.ncbi.nlm.nih.gov), and the initial structure of the molecule was produced by Sybyl 7.3. The geometry of triphenylmethane was subsequently optimized to minimal energy (tolerance of 0.5 kcal mol^{-1}) using the Tripos force field with Gasteiger-Hückel charges,[47] and the lowest energy conformer was utilized for the docking analysis. The Surflex-Dock program which employs an automatic flexible docking algorithm was applied to analyze the possible conformation of the ligand that binds to BSA,[48] and the program PyMOL (http://www.schrodinger.com) was finally used for visualization of the molecular docking results.

Molecular Dynamics Simulation. Molecular dynamics (MD) simulation of BSA-triphenylmethane was performed using Gromacs program, version 4.5.5, with the Gromacs96 54a7 force field.[49,50] Initial conformations of BSA and triphenylmethane were, respectively, taken from the original X-ray diffraction crystal structure that was solved at 2.65 Å resolution (entry codes 4JK4) and the optimal structure originated from molecular docking. The topologies of BSA were generated by Gromacs package directly, whereas triphenylmethane by PRODRG2.5 Server.[51,52] The simulation system was solvated with a periodic cubic box filled with TIP3P water molecules and an approximate number (15) of sodium counterion to neutralize the charge.[53] Totally, there are 47,009 crystallographic solvent molecules, and the shortest distance between the complex and the edge of the box is set to 12 Å. Simulations were carried out using the isothermal-isobaric (NPT) ensemble with an isotropic pressure of 1 bar, and the temperature of the ligand, protein and solvent (water and counterion) was separately coupled to an external bath held at 298 K, using the Berendsen thermostat with 0.1 ps relaxation time.[54-56] The LINCS algorithm was used to constrain bond lengths, and the long-range electrostatic interactions beyond 10.0 Å were modeled using the Particle Mesh Ewald (PME) method with a grid point density of 0.1 nm and an interpolation order of 4.[57-61] A cutoff of 12.0 Å was used for van der Waals' interactions. The MD integration time step was 2.0 fs and covalent bonds were not constrained, and the system configurations were saved every 2.0 ps. To decrease the atomic collisions with each other, both gradient descent and conjugate gradient algorithm were employed to optimize the whole system.[62,63] First the solvated starting structure was preceded by a

1,000-step gradient descent and then by conjugate gradient energy minimization. Subsequently, 500 ps equilibration with position restraints runs to remove possible unfavorable interactions between solute and solvent, and after thorough equilibration, MD simulations were run for 45 ns. Furthermore, the pure protein was also selected to execute a time period (10 ns) MD simulations so as to compare with the first-rank molecular docking complex. The results of MD simulations were finally displayed by Visual Molecular Dynamics 1.9.2,[64,65] and the program Discovery Studio Visualization 4.5 (Accelrys, San Diego, CA) was utilized to show the images of the MD simulations.

Principles of Fluorescence Quenching. Fluorescence quenching refers to any process that decreases the fluorescence intensity of a sample. A variety of molecular interactions can result in quenching, such as excited state reactions, molecular rearrangements, energy transfer, ground state complex formation, and collisional quenching. Fluorescence quenching is described by the well-known Stern-Volmer equation:[66-68]

$$\frac{F_0}{F} = 1 + k_q[Q] = 1 + K_{SV}[Q] \quad (2)$$

In this equation F_0 and F are the fluorescence intensities in the absence and presence of quencher, respectively, k_q is the bimolecular quenching constant, τ_0 is the lifetime of the fluorophore in the absence of quencher, [Q] is the concentration of quencher, and K_{SV} is the Stern-Volmer quenching constant. Therefore equation (2) was used to estimate K_{SV} by linear regression of a plot of F_0/F *versus* [Q].

Calculation of Recognition Ability. When ligand molecules bind independently to a set of equivalent sites on a macromolecule, the equilibrium between free and bound ligand molecules is given by the following relation:[69,70]

$$\log\frac{F_0-F}{F}=n\log K-n\log\frac{1}{[Q_t]-\frac{F_0-F}{F_0}[P_t]} \tag{3}$$

where F_0 and F are the fluorescence intensities in the absence and presence of quencher, respectively, K and n are the association constant and the types of binding sites, respectively, $[Q_t]$ and $[P_t]$ are the total concentration of quencher and protein. Moreover, the fluorescence intensities were corrected for absorption of the exciting light and reabsorption of the emitted light to decrease the inner filter effect by using the following relationship:[39,71]

$$F_{cor}=F_{obs}\times e^{\frac{A_{ex}+A_{em}}{2}} \tag{4}$$

where F_{cor} and F_{obs} are the fluorescence intensities corrected and observed, respectively, and A_{ex} and A_{em} are the absorption of the systems at the excitation and the emission wavelength, respectively. The fluorescence intensity utilized in this work is the corrected intensity.

Time-Resolved Fluorescence. Since the fluorescence lifetime of Trp residue is very sensitive to its molecular environment, determination of the lifetime of Trp residue would reveal much information, such as charge transfer, molecular rotation and quenching of the fluorophore in HSA. The representative fluorescence decay profiles of HSA at various molar ratios of triphenylmethane in Tris-HCl buffer, pH＝7.4, are exhibited in Fig. S1, and the fluorescence lifetime and their amplitudes are also listed in Table S1. Apparently, the fluorescence decay curves fitted excellent to a biexponential function kinetics, which might imply the existence of conformers in equilibrium in the compact structure of HSA. As shown in Table S1, a long (τ_1＝7.29 ns) and a short (τ_2＝3.25 ns) fluorescence lifetime is observed for HSA during the time-resolved fluorescence decay, respectively; whereas in the presence of 80 μM triphenylmethane, the lifetime components are τ_1＝6.08 ns and τ_2＝2.14 ns (χ^2＝1.05). Definitely, the biexponential decay under the circumstances could be attributed to a lone electronic transition of Trp residue, which may present as disparate conformational isomers in the protein.[72-74] In reality, due to steric effects between the side chain of Trp residue and the polypeptide backbone, all rotamers are not completely feasible. The quenching group nearest to the indole moiety is the small amino group upon HSA-triphenylmethane complex formed, accordingly the rotamer with the maximal population and the fluorescence lifetime is 7.29 ns. Conversely, if the amino and carbonyl group close to the indole ring, this rotamer can hold the short fluorescence lifetime of 3.25 ns. Nevertheless, the clarifications of conformers of HSA are just confined to the solution, and the presence of dissimilar Trp residue

rotamers has been independently verified by nuclear magnetic resonance.[75,76] Hence, we have no attention to traverse the individual ingredients of the Trp residue, but instead the average fluorescence lifetime has been employed to receive a qualitative analysis for the exact recognition mechanism between HSA and triphenylmethane. Clearly, the mean fluorescence lifetime of HSA diminishes from 6.04 ns to 5.33 ns, at different concentrations of triphenylmethane, suggesting doubtless that the reduction of Trp residue fluorescence by ligand is primarily static type in nature. In other words, triphenylmethane is patently located within the subdomain IIA on HSA, and the triphenylmethane compound is within neighborhood of the Trp residue throughout the molecular recognition. Although triphenylmethane caused conformational transition in HSA, we should be noted that multiexponential fluorescence decay behavior is generally ascribed to diverse conformations of protein rather than an apportionment to different Trp residues in a protein of one conformation. These results are cohered with the exhaustive explications based on both CD spectra and molecular modeling, and a parallel story has been depicted recently by Banerjee et al.[77] for the investigation of the oxidative interaction between oxyhemoglobin from human blood and adenosine 5'-triphosphate by using different spectroscopic and molecular docking methods.

Stern-Volmer Analyses. As noted earlier, the assessment of fluorescence lifetime is the most definitive approach to acquire the recognition mechanism, however, the steady state fluorescence data can also be processed by the well-known Stern-Volmer equation (2). This operation is able to further explain the recognition reaction and the Stern-Volmer quenching parameters are valuable complement to time-resolved fluorescence decay. Fig. S2 indicates the Stern-Volmer plot of F_0/F *against* [Q] at the four different temperatures, and the calculated K_{SV} and k_q values were collected in Table S2. Intuitively, the linear Stern-Volmer plot Fig. S2 is indicative of a single class of fluorophores, all equally reachable to ligand. Simultaneously, the data in Table S2 show Stern-Volmer quenching constants K_{SV} are inversely correlated with temperature, and the bimolecular quenching constants k_q are roughly 100-fold larger than the typically diffusion-controlled quenching parameter ($\sim 1.0\times10^{10}$ M^{-1} s^{-1}). These outcomes, together with the foregoing fluorescence lifetime data, demonstrates that the molecular recognition of triphenylmethane with HSA is chiefly static interaction (probably 1∶1 association), owing to higher temperature will normally lead to the dissociation of fragilely bound adducts, and thereby smaller amounts of static quenching.

Recognition Capacity and Stoichiometry. To evaluate the recognition ability and stoichiometry of triphenylmethane by HSA, both equation (3) and the method of continuous variation (Job's plot) are adopted in the current situation. The plot of $\log(F_0-F)/F$ *versus* $\log(1/([Q_t]-(F_0-F)[P_t]/F_0))$ for the HSA-triphenylmethane reaction at four different temperatures are emerged in Fig. S3, and the corresponding results of K and n were summarized in Table S2. Evidently, the association constants K are declined with the elevated temperatures, which attested the generation of a weak complex in the HSA-triphenylmethane recognition process, and the frail noncovalent protein-ligand adduct would be in part decomposed when the temperature ascended. In light of the relevant consideration of Mallik et al.,[78] and combined several recently works on the theme of protein-ligand, such as C.I. Basic Violet 4, naproxen, C.I. Acid Yellow 73, retinol, retinoic acid, acremoxanthone C and acremonidin A,[79-83] it is therefore apparent that the molecular recognition of triphenylmethane with HSA falls within the scope of relatively low association with respect to other powerful protein-ligand adducts with recognition capacities ranging from 10^6 to 10^8 M^{-1}.

In two previously publications, via fluorescence spectra, Indig[84] and Zhang et al.[37] narrated respectively that triphenylmethane noncovalently conjugated with BSA having the association constants $K=2.5\times10^4$ M^{-1} and 3.734×10^4 M^{-1}. Although the magnitude of association constant of the HSA-triphenylmethane system (4.159×10^4 M^{-1}) agrees wonderful with the BSA-triphenylmethane complexes, the minute differences exists in the molecular recognition of triphenylmethane by the homologous proteins HSA and BSA, and these distinctions may descend from their

own unique features. Still, the data of *n* is quite close to 1, certifying lucidly the presence of only one single binding site in HSA for triphenylmethane. As we have seen, the peculiar character of intrinsic fluorescence of HSA is due to the sole Trp residue at position 214 (subdomain IIA), from the value of *n*, we ascertain that triphenylmethane binding location is surely close to the aromatic Trp-214 residue, and yielding fluorescence changes in the HSA-triphenylmethane recognition.

The Job's plot is principally used to further substantiate the stoichiometry of the recognition process between HSA and triphenylmethane. In this method, the gross molar concentration of triphenylmethane and HSA are maintained constant, but their molar fractions are changed.[85] Fluorescence emission intensity that is proportional to adduct formation is plotted *against* the molar fractions of these two elements, and the maximum on the plot corresponds to the stoichiometry of the two species. The Job's plot for the HSA-triphenylmethane fluorescence at 339 nm following an excitation at 295 nm is revealed in Fig. S4 and, perceptibly, the *x*-coordinate at the vertex in the picture is nearly 0.52. This result endorses the 1∶1 noncovalent HSA-triphenylmethane complex derived from equation (3), and is also ideally compatible with the stoichiometry of homologous BSA-triphenylmethane reaction expounded by Indig[84] and Zhang et al.,[37] respectively.

Noncovalent Bonds. It is evident to us that the molecular recognition of triphenylmethane by HSA formed a noncovalent HSA-triphenylmethane adduct in the process. Which noncovalent bonds are contributed to the stability of the complex? To answer this question, we need to discuss the energetics and thermodynamic parameters of the present protein-ligand system. In general, the energetics of recognition reactions in solution is expressed in terms of three functions: $\Delta G°$, the Gibbs free energy; $\Delta H°$, the enthalpy; and $\Delta S°$, the entropy. Commonly, there are four types of noncovalent bonds existing in ligand binding biopolymers, that is electrostatic interaction, hydrogen bond, hydrophobic interaction and van der Waals force.[86-88] The sign and magnitude of thermodynamic parameters for enzyme/protein recognition reactions may interpret the acting forces donated to enzyme/protein stability. Suppose the enthalpy $\Delta H°$ does not change significantly over the temperature scope examined, then the three thermodynamic functions are related by equations (5) and (6):

$$\ln K = \frac{-\Delta H^{\circ}}{RT} + \frac{\Delta S^{\circ}}{R} \tag{5}$$

$$\Delta G^{\circ} = \Delta H^{\circ} - T\Delta S^{\circ} \tag{6}$$

In these expressions K is the association constant for a given recognition reaction under a specified set of experimental conditions, R is the gas constant, T is the absolute temperature, and the superscript "°" shows the value of the property of a molar concentration of unity. A linear plot Fig. S5 of ln$K$ *against* 1/T produces $\Delta H°$ and $\Delta S°$, and the data fitted from Fig. S5 were also pooled in Table S2. Plainly, the HSA-triphenylmethane recognition is spontaneous because of the negative value of

$\Delta G°$. In a relatively early review, Ross and Subramanian[89] have generalized the sign and magnitude of the thermodynamic parameters associated with various individual classes of reaction that can occur in enzyme/protein recognition processes. For standard hydrophobic interaction, both $\Delta H°$ and $\Delta S°$ are positive, whereas there are negative for van der Waals force and hydrogen bond formation in low dielectric medium. Specific electrostatic interaction between ionic species in aqueous was communicated by a positive value of $\Delta S°$ and a negative $\Delta H°$ (almost zero). And a negative $\Delta H°$ value is noted whenever there is hydrogen bond in the reaction.[90-92] As for the noncovalent HSA-triphenylmethane adduct, the negative $\Delta H° = -32.08$ kJ mol^{-1} and the negative $\Delta S° = -18.99$ J mol^{-1} K^{-1}, respectively, symbolized explicitly both hydrogen bonds and van der Waals forces play a dominant role in the molecular recognition of triphenylmethane by HSA. Based on the structural quality of triphenylmethane, it owns considerable hydrophobicity as a consequence of cyclic systems; in the meantime, subdomain IIA on HSA is a hydrophobic pocket as well.[93] Thereby we can reasonably deduce that hydrophobic interactions have a remarkable contribution to the molecular recognition of triphenylmethane by HSA; or rather, by strengthening the hydrogen bonds and van der Waals forces the hydrophobic interactions made the noncovalent HSA-triphenylmethane complex more stable.

Competitive Ligand Recognition Studies. The paramount goal of the competitive ligand recognition inquiries was to final validate the recognition patch of triphenylmethane by the HSA molecule. Markedly, pioneering work by Sudlow et al.[94-97] defined two sovereign ligand binding domains on HSA, named site I and site II. Site I is known as the warfarin-azapropazone site, and shaped as a pocket in subdomain IIA, the lone Trp-214 residue of HSA in this region. The inside wall of the domain is formed by hydrophobic side chains, while the entrance to the orifice is surrounded by positively charged residues.[93] The special characteristic of this site is the binding of the ligand, which is a bulky heterocyclic anion with the charge situated in a fairly central position in the molecule.[98] Typically site I ligand include azapropazone, diflunisal, phenylbutazone and warfarin.[99,100] Site II corresponds to the cavity of subdomain IIIA, and is also known as the indole-benzodiazepine site, which is almost the same size as site I, the interior of the hole is constituted by hydrophobic amino acid residues and the exterior patch presented two significant amino acid residues, i.e. Arg-410 and Tyr-411.[101] Ligands binding to site II are generally aromatic and may be neutral; a charge, if present, is anionic and located more peripherally on the molecule, such as flufenamic acid, halothane, ibuprofen and naproxen.[102,103] Subsequently Brodersen et al.[104] clearly designated that digitoxin binding in HSA is independent from Sudlow's site, and perch on what was nominated as site III. In the current study, the competitors used included phenylbutazone, a classical marker for site I, flufenamic acid for site II, and digitoxin for site III. According to the protocol, the recognition capacity of triphenylmethane by HSA in

the presence of different site markers were fitted from fluorescence data and observed to be 0.5095×10^4 M^{-1}, 3.951×10^4 M^{-1} and 4.018×10^4 M^{-1} for phenylbutazone, flufenamic acid and digitoxin, respectively. Without any question, the molecular recognition of triphenylmethane with HSA was mostly inhibited by phenylbutazone, or triphenylmethane shares the same pocket with phenylbutazone in HSA. These phenomena confirm convincingly that our previous conclusion based on steady-state and time-resolved fluorescence and stoichiometric analysis is logical and is also entirely tying in with the elaborate perorations of molecular modeling.

Conformational Stability. After the examinations of time-resolved fluorescence, one can discover that the conformation of HSA has changed to a certain degree in the HSA-triphenylmethane recognition process. In order to survey the conformational alterations of HSA quantitatively, the far-UV circular dichroism (CD) spectra of protein in the absence and presence of triphenylmethane were recorded in Fig. S6, and the secondary structure components estimated based on raw CD data gathered in Table S3. Vividly, the CD curve of HSA appeared two negative bands in the far-UV CD region at 208 nm and 222 nm, feature of α-helical structure of globular proteins. The rational elucidation is that the negative peaks between 208 and 209 nm and 222 and 223 nm are both contributed by $\pi\rightarrow\pi^*$ and $n\rightarrow\pi^*$ transition for the peptide bond of α-helix.[105,106] Table S3 manifests free HSA has 59.3% α-helix, 7.4% β-sheet, 11.8% turn and 21.5% random coil, upon complex with triphenylmethane, diminution of α-helix was perceived from 59.3% free HSA to 51.2% HSA-triphenylmethane adduct; and concurrently growth in β-sheet, turn and random coil from 7.4%, 11.8% and 21.5% free HSA to 9.2%, 14.2% and 25.4% HSA-triphenylmethane at a molar ratio of HSA to triphenylmethane of 1∶4. The decrease of α-helix with the expansion in the β-sheet, turn and random coil divulges obviously that triphenylmethane conjugated with amino acid residues of the polypeptide chain and ultimately yields the transition of the HSA conformation, e.g. some extent of protein destabilization upon triphenylmethane recognition.[107] We should also bear in mind that the conformational transition of HSA in such conditions does not mean seriously destroy the orderly spatial conformation of protein, but the self-regulation of HSA so as to accommodate the triphenylmethane

compound more firmly. In fact, HSA is not in a stationary state, per contra the complete protein tumbles in around 40 ns and quickly altering in shape. The major reason for this phenomenon is that the loop link structure allows HSA fast distention, shrinkage, and flexion, some of it inherent and some are related to recognition of ligands.[108,109] Furthermore, components of HSA are ceaselessly moving on more rapid time ranges. And this view has been supported by Munro et al.,[110] who exploited time-resolved fluorescence to detect the motion of side chain of Trp residue on HSA, and the consequence disclosed clearly that the side chain of Trp residue rotates individually at a swift rate (10^{-10} s). Therefore, HSA in solution may be regarded as possessing a simple heart-shaped general, but it is realistically to consider it as an assemblage of peristaltic, flexible segments, frequently transition in conformation via splaying and shutting of dominant fissures. With this pattern resembling respiration, and with many of its amino acid residues side chains continually in motion on a microscale, HSA is well fitted to incorporate or discharge various ligands such as triphenylmethane that it influences the biological profiles of these substances in the human body.

Table S1
Fluorescence lifetimes of HSA as a function of concentrations of triphenylmethane

c(triphenylmethane) (μM)	τ_1 (ns)	τ_2 (ns)	A_1	A_2	τ (ns)	χ^2
0	3.25	7.29	0.31	0.69	6.04	1.09
10	3.03	7.14	0.29	0.71	5.95	1.01
20	2.76	6.88	0.25	0.75	5.85	0.98
40	2.65	6.82	0.24	0.76	5.82	1.12
80	2.14	6.08	0.19	0.81	5.33	1.05

Table S2
Recognition parameters and thermodynamic functions for the HSA-triphenylmethane system at different temperatures

T (K)	K_{SV} ($\times 10^4$ M^{-1})	k_q ($\times 10^{12}$ M^{-1} s^{-1})	R^a	K ($\times 10^4$ M^{-1})	n	R^a	$\Delta H°$ (kJ mol^{-1})	$\Delta G°$ (kJ mol^{-1})	$\Delta S°$ (J mol^{-1} K^{-1})
298	4.916	8.139	0.9996	4.159	0.98	0.9995	−32.08	−26.35	−18.99
303	4.496	7.444	0.9998	3.548	0.97	0.9995		−26.39	
308	4.085	6.763	0.9996	2.884	0.97	0.9996		−26.30	
313	3.759	6.224	0.9993	2.234	0.95	0.9996		−26.06	

[a] R is the correlation coefficient.

Table S3

Secondary structure components (CD spectra) of HSA conjugates with triphenylmethane at pH＝7.4 assessed by Jasco Spectra Manager II Software

c(triphenylmethane) (μM)	Secondary structure components (%)			
	α-helix	β-sheet	Turn	Random
0	59.3	7.4	11.8	21.5
10	55.5	8.1	12.9	23.5
20	51.2	9.2	14.2	25.4

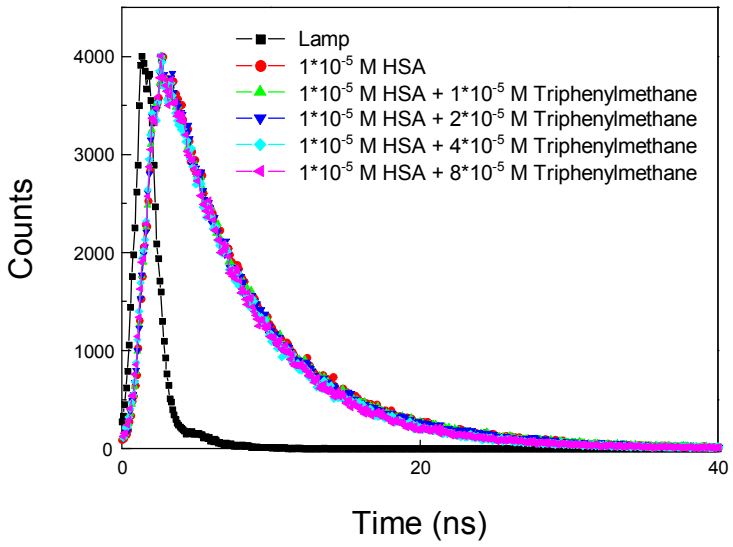

Fig. S1. Time-resolved fluorescence decays of HSA in Tris-HCl buffer (pH＝7.4) as a function of triphenylmethane concentrations. *c*(HSA)＝10 μM, *c*(triphenylmethane)＝0 (red), 10 (green), 20 (blue), 40 (cyan) and 80 (magenta) μM. The sharp pattern on the left (black) is the lamp profile.

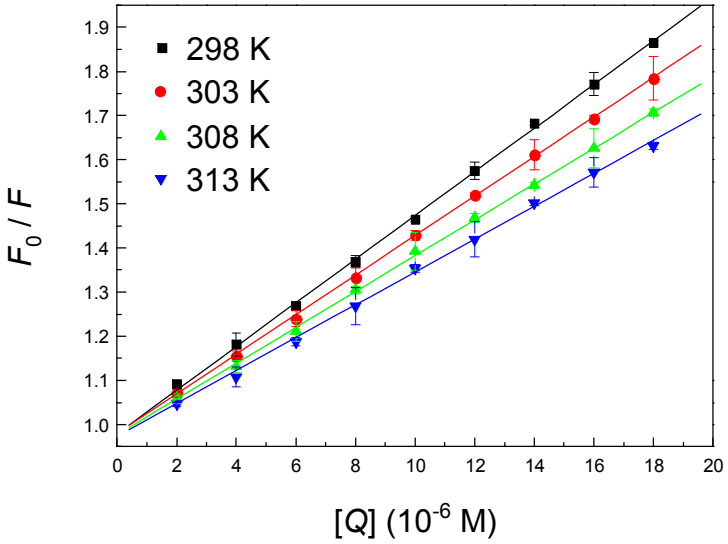

Fig. S2. Stern-Volmer plot showing Trp-214 residue quenching of HSA at pH＝7.4 in the presence of different amounts of triphenylmethane. *c*(HSA)＝1.0 μM, *c*(triphenylmethane)＝2.0, 4.0, 6.0, 8.0, 10, 12, 14, 16 and 18 μM. Each point was the mean of three independent determinations±S.D. ranging 0.46%－4.94%.

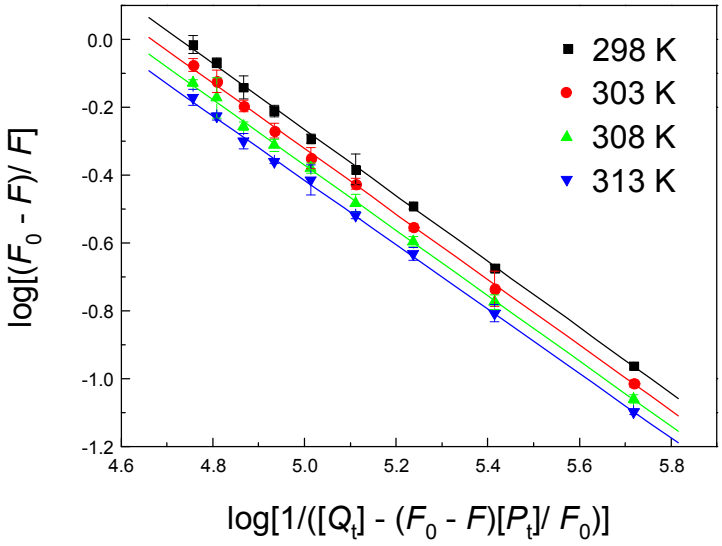

Fig. S3. Recognition capacity plot explaining Trp-214 residue quenching of HSA (1.0 μM) at pH＝7.4 induced by triphenylmethane molecular recognition. The fluorescence intensity was read at λ_{ex}＝295 nm and the λ_{em} maximum occurred at 349 nm. Each data was the average of three separate experiments±S.D. ranging 0.7%—5.94%.

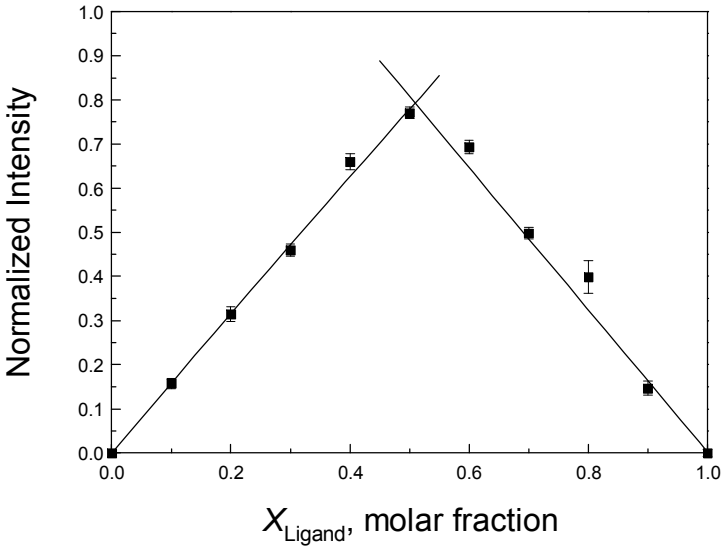

Fig. S4. Job's plot for HSA-triphenylmethane fluorescence based on the method of continuous variation (pH＝7.4, *T*＝298 K). All data were corrected for triphenylmethane fluorescence and each value was the mean of three respective observations±S.D. ranging 0.76%－3.71%.

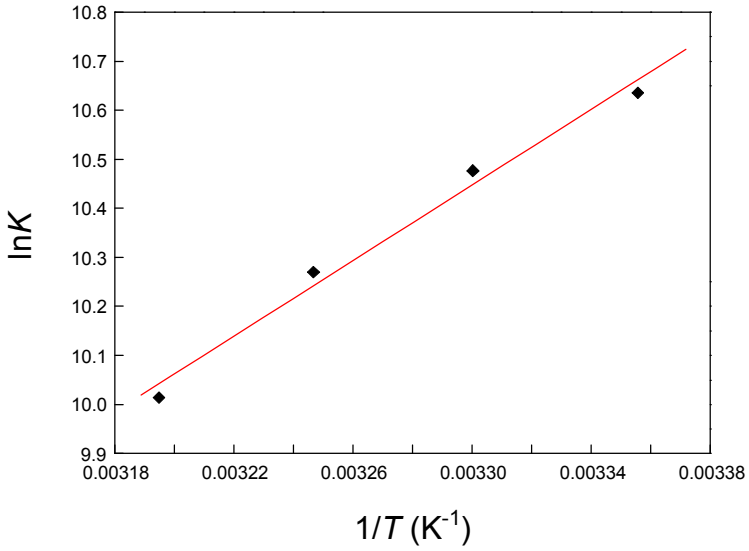

Fig. S5. van't Hoff plot for the recognition reaction between HSA and triphenylmethane in Tris-HCl buffer, pH＝7.4; y＝3858x－2.284, R＝0.993.

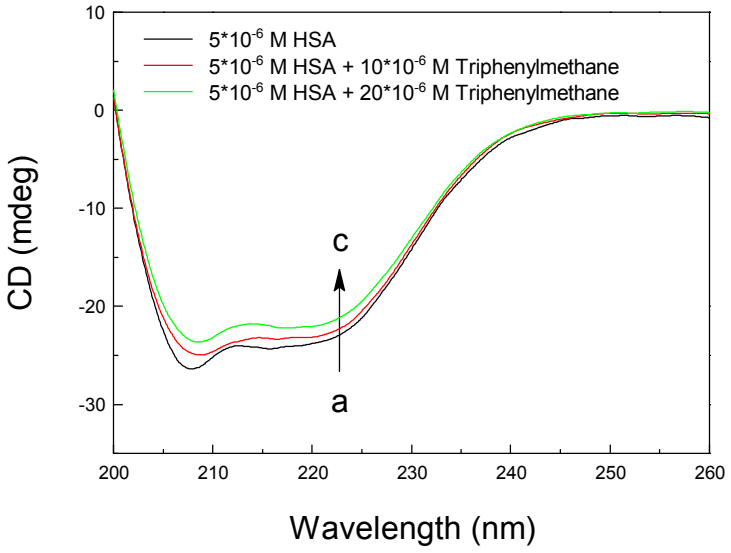

Fig. S6. Far-UV CD spectra of the HSA-triphenylmethane adduct at pH＝7.4 and T＝298 K, 5.0 μM HSA in the presence of 0 (black), 10 (red) and 20 (green) μM triphenylmethane.

References

1. T. Gessner and U. Mayer, in *Ullmann's Encyclopedia of Industrial Chemistry*, ed. M. Bohnet and F. Ullmann, John Wiley & Sons, Inc., Hoboken, NJ, 6th edn., 2000, vol. 37, pp 425-478.
2. D. Thetford and Updated by Staff, in *Kirk-Othmer Encyclopedia of Chemical Technology*, ed. A. Seidel, John Wiley & Sons, Inc., Hoboken, NJ, 5th edn., 2013, vol. 24, pp 1-19.
3. D. J. Alderman, *J. Fish Dis.*, 1985, **8**, 289-298.
4. D. J. Alderman and R. S. Clifton-Hadley, *Vet. Rec.*, 1988, **122**, 103-106.
5. P. Kovacic and R. Somanathan, *J. Appl. Toxicol.*, 2014, **34**, 825-834.
6. S. Srivastava, R. Sinha and D. Roy, *Aquat. Toxicol.*, 2004, **66**, 319-329.
7. N. A. Botsoglou and D. J. Fletouris, in *Drug Residues in Foods: Pharmacology, Food Safety, and Analysis*, CRC Press, Boca Raton, FL, 2000, pp 211-489.
8. R. Naylor and M. Burke, *Annu. Rev. Environ. Resour.*, 2005, **30**, 185-218.
9. T. Reyns, C. Belpaire, C. Geeraerts and J. V. Loco, *J. Chromatogr. B: Anal. Technol. Biomed. Life Sci.*, 2014, **953-954**, 92-101.
10. S. Clemmensen, J. C. Jensen, N. J. Jensen, O. Meyer, P. Olsen and G. Würtzen, *Arch. Toxicol.*, 1984, **56**, 43-45.
11. K. V. K. Rao, *Toxicol. Lett.*, 1995, **81**, 107-113.
12. S. J. Culp and F. A. Beland, *J. Am. Coll. Toxicol.*, 1996, **15**, 219-238.

13. S. J. Culp, L. R. Blankenship, D. F. Kusewitt, D. R. Doerge, L. T. Mulligan and F. A. Beland, *Chem.-Biol. Interact.*, 1999, **122**, 153-170.

14. H. Spiller, G. Rodgers, D. Willias, G. Bosse and J. Sullivan, *Clin. Toxicol.*, 2008, **46**, 320-321.

15. S. M. Donya, A. A. Farghaly, M. A. Abo-Zeid, H. F. Aly, S. A. Ali, M. A. Hamed and N. S. El-Rigal, *Eur. Rev. Med. Pharmacol. Sci.*, 2012, **16**, 469-482.

16. C. Fernandes, V. S. Lalitha and K. V. K. Rao, *Carcinogenesis*, 1991, **12**, 839-845.

17. F. P. Meyer and T. A. Jorgenson, *Trans. Am. Fish. Soc.*, 1983, **112**, 818-824.

18. http://ntp.niehs.nih.gov/ntp/htdocs/LT_rpts/tr527.pdf

19. Z. S. Chen, H. B. Deng, C. Chen, Y. Yang and H. Xu, *J. Environ. Health Sci. Eng.*, 2014, **12**, 63.

20. D. Briggs, *Br. Med. Bull.*, 2003, **68**, 1-24.

21. V. Carbone and T. Velkov, *Chem. Res. Toxicol.*, 2013, **26**, 1240-1250.

22. M. G. Allmark, W. A. Mannell and H. C. Grice, *J. Pharm. Pharmacol.*, 1957, **9**, 622-628.

23. W. J. Rea, *J. Nutr. Environ. Med.*, 1996, **6**, 55-124.

24. K. Kümmerer, *Annu. Rev. Environ. Resour.*, 2010, **35**, 57-75.

25. Z. Y. Guo, P. P. Gai, T. T. Hao, J. Duan and S. Wang, *J. Agric. Food Chem.*, 2011, **59**, 5257-5262.

26. F. Y. Liu, X. Yang, Y. Q. Zhao and S. G. Sun, *Anal. Methods*, 2013, **5**, 660-665.

27. N. López-Gutiérrez, R. Romero-González, J. L. M. Vidal and A. G. Frenich, *Anal. Methods*, 2013, **5**, 3434-3449.

28. D. Hurtaud-Pessel, P. Couëdor, E. Verdon and D. Dowell, *J. AOAC Int.*, 2013, **96**, 1152-1157.

29. J.-X. Dong, C. Xu, H. Wang, Z.-L. Xiao, S. J. Gee, Z.-F. Li, F. Wang, W.-J. Wu, Y.-D. Shen, J.-Y. Yang, Y.-M. Sun and B. D. Hammock, *J. Agric. Food Chem.*, 2014, **62**, 8752-8758.

30. Y. Y. Zhang, W. S. Yu, L. Pei, K. Q. Lai, B. A. Rasco and Y. Q. Huang, *Food Chem.*, 2015, **169**, 80-84.

31. M. J. Schneider and W. C. Andersen, *J. AOAC Int.*, 2015, **98**, 658-670.

32. Y. Wang and L. G. Chen, *J. Chromatogr. B: Anal. Technol. Biomed. Life Sci.*, 2015, **1002**, 98-106.

33. G. L. Indig, D. G. Jay and J. J. Grabowski, *Biophys. J.*, 1992, **61**, 631-638.

34. J. A. Bartlett and G. L. Indig, *Dyes Pigm.*, 1999, **43**, 219-226.

35. I. Özer and A. Çağlar, *Dyes Pigm.*, 2002, **54**, 11-16.

36. Y. Eldem and I. Özer, *Dyes Pigm.*, 2004, **60**, 49-54.

37. Y.-Z. Zhang, B. Zhou, X.-P. Zhang, P. Huang, C.-H. Li and Y. Liu, *J. Hazard. Mater.*, 2009, **163**, 1345-1352.

38. G. F. Li, D. Magana and R. B. Dyer, *Nat. Commun.*, 2014, **5**, 3100.

39. J. R. Lakowicz, in *Principles of Fluorescence Spectroscopy*, Springer Science+Business Media, New York, NY, 3rd edn., 2006, pp 63-606.

40. O. K. Abou-Zied, *RSC Adv.*, 2013, **3**, 8747-8755.

41. O. K. Abou-Zied, N. I. Zahid, M. F. Khyasudeen, D. S. Giera, J. C. Thimm and R. Hashim, *Sci. Rep.*, 2015, **5**, 8699.

42. A. Bujacz, *Acta Crystallogr. Sect. D: Biol. Crystallogr.*, 2012, **68**, 1278-1289.

43. K. A. Majorek, P. J. Porebski, A. Dayal, M. D. Zimmerman, K. Jablonska, A. J. Stewart, M. Chruszcz and W. Minor, *Mol. Immunol.*, 2012, **52**, 174-182.

44. B. Sekula, K. Zielinski and A. Bujacz, *Int. J. Biol. Macromol.*, 2013, **60**, 316-324.

45. A. Bujacz, K. Zielinski and B. Sekula, *Proteins: Struct. Funct. Bioinformatics*, 2014, **82**, 2199-2208.

46. S. J. Weiner, P. A. Kollman, D. T. Nguyen and D. A. Case, *J. Comput. Chem.*, 1986, **7**, 230-252.

47. M. Clark, R. D. Cramer III and N. van Opdenbosch, *J. Comput. Chem.*, 1989, **10**, 982-1012.

48. A. E. Cleves and A. N. Jain, *J. Comput.-Aided Mol. Des.*, 2015, **29**, 485-509.

49. C. Oostenbrink, A. Villa, A. E. Mark and W. F. van Gunsteren, *J. Comput. Chem.*, 2004, **25**, 1656-1676.

50. B. Hess, C. Kutzner, D. van der Spoel and E. Lindahl, *J. Chem. Theory Comput.*, 2008, **4**, 435-447.

51. A. W. Schüttelkopf and D. M. F. van Aalten, *Acta Crystallogr. Sect. D: Biol. Crystallogr.*, 2004, **60**, 1355-1363.

52. M. Lundborg and E. Lindahl, *J. Phys. Chem. B*, 2015, **119**, 810-823.

53. W. L. Jorgensen, J. Chandrasekhar, J. D. Madura, R. W. Impey and M. L. Klein, *J. Chem. Phys.*, 1983, **79**, 926-935.

54. K. Ikeda, *Prog. Theor. Phys.*, 1967, **38**, 584-610.

55. H. J. C. Berendsen, J. P. M. Postma, W. F. van Gunsteren, A. DiNola and J. R.

Haak, *J. Chem. Phys.*, 1984, **81**, 3684-3690.

56. A. D. Nola, H. J. C. Berendsen and O. Edholm, *Macromolecules*, 1984, **17**, 2044-2050.
57. R. Edberg, D. J. Evans and G. P. Morriss, *J. Chem. Phys.*, 1986, **84**, 6933-6939.
58. A. Baranyai and D. J. Evans, *Mol. Phys.*, 1990, **70**, 53-63.
59. B. Hess, H. Bekker, H. J. C. Berendsen and J. G. E. M. Fraaije, *J. Comput. Chem.*, 1997, **18**, 1463-1472.
60. T. Darden, D. York and L. Pedersen, *J. Chem. Phys.*, 1993, **98**, 10089-10092.
61. T. Darden, L. Perera, L. P. Li and L. Pedersen, *Structure*, 1999, **7**, R55-R60.
62. J. A. Snyman, in *Practical Mathematical Optimization: An Introduction to Basic Optimization Theory and Classical and New Gradient-Based Algorithms*, Springer Science＋Business Media, New York, NY, 2005, vol. 97, pp 1-150.
63. M. R. Hestenes and E. Stiefel, *J. Res. Natl. Bur. Stand.*, 1952, **49**, 409-436.
64. W. Humphrey, A. Dalke and K. Schulten, *J. Mol. Graph.*, 1996, **14**, 33-38.
65. J. Hsin, A. Arkhipov, Y. Yin, J. E. Stone and K. Schulten, *Curr. Protoc. Bioinformatics*, 2008, **24**, 5.7.1-5.7.48.
66. O. Stern and M. Volmer, *Phys. Z.*, 1919, **20**, 183-188.
67. N. Zaidi, E. Ahmad, M. Rehan, G. Rabbani, M. R. Ajmal, Y. Zaidi, N. Subbarao and R. H. Khan, *J. Phys. Chem. B*, 2013, **117**, 2595-2604.
68. B. P. Pahari, S. Chaudhuri, S. Chakraborty and P. K. Sengupta, *J. Phys. Chem. B*, 2015, **119**, 2533-2545.
69. S. Y. Bi, L. Ding, Y. Tian, D. Q. Song, X. Zhou, X. Liu and H. Q. Zhang, *J. Mol.*

Struct., 2004, **703**, 37-45.

70. S. Y. Bi, D. Q. Song, Y. Tian, X. Zhou, Z. Y. Liu and H. Q. Zhang, *Spectrochim. Acta Part A: Mol. Biomol. Spectrosc.*, 2005, **61**, 629-636.
71. M. Kallubai, A. Rachamallu, D. P. Yeggoni and R. Subramanyam, *Mol. BioSyst.*, 2015, **11**, 1172-1183.
72. J. R. Lakowicz, *Photochem. Photobiol.*, 2000, **72**, 421-437.
73. O. J. Rolinski, A. Martin and D. J. S. Birch, *Ann. N. Y. Acad. Sci.*, 2008, **1130**, 314-319.
74. L. Brancaleon, *Adv. Protein Chem. Struct. Biol.*, 2013, **93**, 95-152.
75. J. M. Beechem and L. Brand, *Annu. Rev. Biochem.*, 1985, **54**, 43-71.
76. S. L. C. Moors, A. Jonckheer, M. D. Maeyer, Y. Engelborghs and A. Ceulemans, *Curr. Protein Pept. Sci.*, 2008, **9**, 427-446.
77. M. Banerjee, A. Chakrabarti and S. Basu, *J. Phys. Chem. B*, 2012, **116**, 6150-6157.
78. R. Mallik, M. J. Yoo, C. J. Briscoe and D. S. Hage, *J. Chromatogr. A*, 2010, **1217**, 2796-2803.
79. M. S. Baptista and G. L. Indig, *J. Phys. Chem. B*, 1998, **102**, 4678-4688.
80. T. Banerjee, S. K. Singh and N. Kishore, *J. Phys. Chem. B*, 2006, **110**, 24147-24156.
81. N. Barbero, E. Barni, C. Barolo, P. Quagliotto, G. Viscardi, L. Napione, S. Pavan and F. Bussolino, *Dyes Pigm.*, 2009, **80**, 307-313.
82. A. Belatik, S. Hotchandani, J. Bariyanga and H. A. Tajmir-Riahi, *Eur. J. Med.*

Chem., 2012, **48**, 114-123.

83. A. Madariaga-Mazón, M. González-Andrade, M. del C. González, A. E. Glenn, C. M. Cerda-García-Rojas and R. Mata, *J. Nat. Prod.*, 2013, **76**, 1454-1460.
84. G. L. Indig, in *Optical Methods for Tumor Treatment and Detection: Mechanisms and Techniques in Photodynamic Therapy V*, ed. T. J. Dougherty, SPIE, Bellingham, WA, 1996, vol. 2675, pp 228-237.
85. E. J. Olson and P. Bühlmann, *J. Org. Chem.*, 2011, **76**, 8406-8412.
86. M. T. Record Jr, C. F. Anderson and T. M. Lohman, *Q. Rev. Biophys.*, 1978, **11**, 103-178.
87. R. Perozzo, G. Folkers and L. Scapozza, *J. Recept. Signal Transduct.*, 2004, **24**, 1-52.
88. J. B. Chaires, *Annu. Rev. Biophys.*, 2008, **37**, 135-151.
89. P. D. Ross and S. Subramanian, *Biochemistry*, 1981, **20**, 3096-3102.
90. P. D. Ross and S. Subramanian, *Biophys. J.*, 1980, **32**, 79-81.
91. H.-J. Hinz, *Annu. Rev. Biophys. Bioeng.*, 1983, **12**, 285-317.
92. J. D. Chodera and D. L. Mobley, *Annu. Rev. Biophys.*, 2013, **42**, 121-142.
93. D. C. Carter and J. X. Ho, *Adv. Protein Chem.*, 1994, **45**, 153-203.
94. G. Sudlow, D. J. Birkett and D. N. Wade, *Mol. Pharmacol.*, 1973, **9**, 649-657.
95. G. Sudlow, D. J. Birkett and D. N. Wade, *Clin. Exp. Pharmacol. Physiol.*, 1975, **2**, 129-140.
96. G. Sudlow, D. J. Birkett and D. N. Wade, *Mol. Pharmacol.*, 1975, **11**, 824-832.
97. G. Sudlow, D. J. Birkett and D. N. Wade, *Mol. Pharmacol.*, 1976, **12**, 1052-1061.

98. T. Peters Jr., in *All about Albumin: Biochemistry, Genetics, and Medical Applications*, Academic Press, San Diego, CA, 1995, pp 9-132.

99. I. Petitpas, A. A. Bhattacharya, S. Twine, M. East and S. Curry, *J. Biol. Chem.*, 2001, **276**, 22804-22809.

100. D. C. Carter, in *Burger's Medicinal Chemistry and Drug Discovery*, ed. D. J. Abraham and D. P. Rotella, John Wiley & Sons, Inc., Hoboken, NJ, 7th edn., 2010, pp 437-467.

101. T. Peters Jr., *Adv. Protein Chem.*, 1985, **37**, 161-245.

102. J. Ghuman, P. A. Zunszain, I. Petitpas, A. A. Bhattacharya, M. Otagiri and S. Curry, *J. Mol. Biol.*, 2005, **353**, 38-52.

103. T. Wybranowski, M. Cyrankiewicz, B. Ziomkowska and S. Kruszewski, *BioSystems*, 2008, **94**, 258-262.

104. R. Brodersen, T. Sjödin and I. Sjöholm, *J. Biol. Chem.*, 1977, **252**, 5067-5072.

105. J. F. Towell III and M. C. Manning, in *Analytical Applications of Circular Dichroism*, ed. N. Purdie and H. G. Brittain, Elsevier B.V., Amsterdam, The Netherlands, 1994, vol. 14, pp 175-205.

106. L. Whitmore and B. A. Wallace, *Biopolymers*, 2008, **89**, 392-400.

107. D. Charbonneau, M. Beauregard and H.-A. Tajmir-Riahi, *J. Phys. Chem. B*, 2009, **113**, 1777-1784.

108. C. Domonkos, I. Fitos, J. Visy and F. Zsila, *Phys. Chem. Chem. Phys.*, 2014, **16**, 22632-22642.

109. G. Pescitelli, L. D. Bari and N. Berova, *Chem. Soc. Rev.*, 2014, **43**, 5211-5233.

110. I. Munro, I. Pecht and L. Stryer, *Proc. Natl. Acad. Sci. U. S. A.*, 1979, **76**, 56-60.